The structure of molten $DyCl_3$ and $DyNa_3Cl_6$ simulated with polarizable- and rigid-ion models

1999 J. Phys.: Condens. Matter 11 645

(http://iopscience.iop.org/0953-8984/11/3/005)

J. Phys.: Condens. Matter **11** (1999) 645–658. Printed in the UK PII: S0953-8984(99)98094-3

The structure of molten $DyCl_3$ and $DyNa_3Cl_6$ simulated with polarizable- and rigid-ion models

Ryuzo Takagi†, Francis Hutchinson‡, Paul A Madden‡, Ashok K Adya§ and Marcelle Gaune-Escard‖

† Research Laboratory for Nuclear Reactors, Tokyo Institute of Technology, Ookayama, Meguro-ku, Tokyo 152-0033, Japan
‡ Physical and Theoretical Chemistry Laboratory, University of Oxford, South Parks Road, Oxford OX1 3QZ, UK
§ Division of Applied Chemistry, School of Molecular and Life Sciences, University of Abertay Dundee, Bell Street, Dundee DD1 1HG, UK
‖ IUSTI, CNRS-UMR 6595, Technopole de Chatau-Gombert, 5 rue Enrico Fermi, 13453 Marseille Cédex 13, France

Received 5 October 1998

Abstract. Molecular dynamics (MD) simulations of molten $DyCl_3$ were carried out using the polarizable-ion model (PIM) and the rigid-ion model (RIM). In these simulations the Born–Mayer–Huggins potential was employed with the same potential parameters for both models. In the PIM the polarization of the chloride ions was supplemented. Although the partial radial distribution functions (rdfs) between Dy and Cl, and between Cl and Cl are very similar for the two models, the rdf between Dy and Dy is quite different. The rdf between Dy and Dy experimentally determined by the isotope substitution method was well reproduced by the PIM. The strong Coulomb interaction between Dy^{3+} and Dy^{3+} is screened by the polarization of Cl^- ions and the interaction distance between Dy^{3+} and Dy^{3+} becomes smaller than that given by the RIM.

MD simulations for $DyNa_3Cl_6$ were made similarly. The PIM also reproduced the experimental total structure factor very well.

1. Introduction

The trivalent metal chlorides present a challenging class of systems as regards modelling the interatomic interactions [1]. Some systems, such as lanthanum chloride, exhibit a strongly ionic character—a charge-ordered crystal which melts at high temperature with a substantial change of molar volume to form an ionically conducting melt. The remainder of the lanthanides also form trivalent chlorides but the conductivity of the melt gradually diminishes across the lanthanide series, along with the ionic radius. Other elements which form chemically similar trivalent cations (in the sense that they have rare-gas outer electron configurations, the open f shells of the lanthanides being buried in the core) include yttrium, scandium and aluminium. These extend the range of ionic radii still further. Whereas YCl_3 has similar properties to some of the lighter lanthanides (like $ErCl_3$ and $TmCl_3$), Sc^{3+} and Al^{3+} have very small ionic radii and their chlorides exhibit distinctively 'covalent' properties, such as low melting point, high vapour pressure and a very low conductivity in the molten phase. The challenge offered is to understand the transition in the behaviour of these (chemically) closely related systems from 'ionic' to 'covalent' with a unified description of the interionic interactions and to detail the change in the microscopic structure of the materials which is responsible for this behaviour.

0953-8984/99/030645+14$19.50

In recent work [2], it has been shown how a fundamentally ionic interaction model is capable of accounting for a much wider range of 'covalent' behaviour than had hitherto been suspected. An ionic interaction model has formal charges on the ions and includes only those interactions which are appropriate to closed-shell species [3]—short-range repulsion, dispersion, induction (or polarization) and charge–charge interactions. The important concept, which allows for the enhanced range of applicability compared to ionic pair potentials, is that an ion's properties are enormously affected by the instantaneous environment in which it finds itself in the course of thermal motion and that this gives *many-body* character to the effective interactions. The induction of multipoles, giving rise to the polarization interactions, is one such effect [4]. Others include the 'breathing' of an ion [5], which gives a coordination-number-dependent contribution to the effective interactions. Polarization effects have been shown to play an important role in accounting for the properties of halide systems; in particular, for the prevalence of layered crystals in MX_2 systems [6] and in determining the morphology of the networks [7, 8] which form in their melts (controlling M–X–M bond angles and the degree of edge or corner sharing of the network polyhedra). Breathing effects are found to be very important for oxides, but much less so for halides [9].

An important motivation for pursuing the development of a generalized ionic model is that, if applicable, the potentials should be highly *transferable.* One aspect of transferability is that a potential developed for one material should be closely related to that of a chemically similar one. For the MCl_3 systems, we have developed a 'generic' series of potentials which differ only in the cation radius. A problem with validating these potentials has been that although the macroscopic properties of the melts (conductivity etc) have been well studied, there is little *direct* experimental evidence about their structure at the atomistic level. *Total* neutron and x-ray diffraction measurements have been made for some systems [10, 11] but, until recently, no isotopically resolved partial structure factors have been measured. In network-forming melts, an important aspect of the structure is the way that the local coordination polyhedra, expected to be $LnCl_6^{3-}$ octahedra for the lanthanide chlorides, are connected together (say, by edge or corner sharing) and this will be most strongly reflected in the cation–cation partial. Very recently, Adya *et al* have reported neutron results for three samples of molten $DyCl_3$ with different isotopic compositions and have used them to separate partial structure factors and radial distribution functions [12]. In this paper, therefore, we compare the structures predicted by the generic simulation model, with a cation radius appropriate to Dy^{3+}, with this new experimental information for $DyCl_3$. As we shall see, the comparison provides direct evidence for the importance of polarization effects in determining the structure of these melts, similar to that already detailed for MX_2 systems.

A second aspect of transferability is that an ionic potential which describes a binary system should transfer unchanged to describe the same set of interactions in a mixture. To describe the properties of mixtures and the complex ions which form within them is an important

Table 1. Potential parameters.

Ion pair	a_{ij}/au	B_{ij}/au	C_{ij}^6/au	b/au
Cl–Cl	1.26	36.44	200	1.34
Dy–Cl	2.44	4008.61	0	—
Na–Cl	1.67	71.71	0	—
Dy–Dy	37.8	0	0	—
Na–Dy	4.64	3.8×10^6	0	—
Na–Na	2.47	317.55	0	—

goal of research on these melts, as complex ion formation has an important effect on the thermodynamic and transport properties and influences purification and extraction processes. We will therefore compare with the experimental total structure factor predicted for a molten mixture of composition $DyNa_3Cl_6$ from a simulation in which we have combined the $DyCl_3$ interaction potential with a well-established potential describing the NaCl interactions.

2. Computational procedure

The potentials used in the present work consist of Born–Mayer–Huggins pair potentials to describe the short-range repulsion, dispersion and charge–charge interactions:

$$\phi_{ij} = Q_i Q_j / r_{ij} + A_{ij} \exp(-a_{ij}(r_{ij} - \sigma_i - \sigma_j)) - C_{ij}^6 / r_{ij}^6 \tag{2.1}$$

supplemented by an account of polarization effects via the polarizable-ion model introduced previously (PIM) [4]. Each ion in the potential is described by a formal charge, Q_i, an effective radius, σ_i, and an effective hardness parameter, ρ_i.

In order to highlight the consequences of the polarization effects, we will contrast the PIM-predicted behaviour with that of the pair potential alone—dubbed the RIM (rigid-ion model). Parameters are listed in table 1, where $a_{ij} = 1/(\rho_i + \rho_j)$ and $B_{ij} = A_{ij} \exp(a_{ij}(\sigma_i + \sigma_j))$. For the repulsive part of the pair potential the parameters are very similar to those suggested by Taltipinar *et al* for a MCl_3 system [1]. The dispersion terms are calculated from the ionic polarizabilities by using the Slater–Kirkwood relationship [13]. For the polarizabilities we use $a_{Cl^-} = 20$ au, the in-crystal Cl^- polarizability for NaCl [14], and $a_{Dy^+} = 10$ au, a characteristic Ln^{3+} value obtained from the refractive indices of their crystalline fluorides by subtracting the anion contribution. However, since the repulsive interactions are dominated by the Coulombic term for all cation–cation combinations, the cation–cation dispersion terms are neglected. The long-range Coulomb interaction was estimated by the Ewald method.

Only the Cl^- ion is treated as polarizable in calculating the polarization contributions to the interionic forces. We have shown that polarization of Ln^{3+} ions is unimportant as they tend to sit in symmetrical (octahedral) coordination environments [11]. The polarization effects are additionally affected by the induction dumping parameter b [4], which is determined from the cation radius through $b = c/(\sigma_{Cl^-} + \sigma_{Dy^{3+}})$, where $c = 7.42$ has the same value for all $LnCl_3$ systems.

The simulations contained 125 Dy^{3+} and 375 Cl^- ions for $DyCl_3$ and 50 Dy^{3+}, 150 Na^+ and 300 Cl^- ions for $DyNa_3Cl_6$ in the PIM and the RIM system. They were run close to the experimental melting temperature and the simulation cell length was estimated from the experimental density [15]. The systems were well annealed, then data acquisitions were made for 10^4 time steps. Total structure factors were estimated by the Fourier transformation of the partial radial distribution functions (rdfs). For small values of the transform variable (k), such transforms become unreliable because of truncation errors in the rdfs and therefore we directly calculate the structure factor from

$$S(k) = \left\langle N^{-1} \sum \mathrm{e}^{\mathrm{i}\boldsymbol{k}\boldsymbol{r}_{ij}} \right\rangle$$

for those vectors $\boldsymbol{k}$ which are consistent with the periodic boundary conditions.

3. Results for $DyCl_3$

3.1. Real-space structure

Partial rdfs obtained with PIM and RIM potentials are compared in figures 1(a)–1(c) with those obtained from Fourier transforms of the neutron partial structure factors. The g_{Dy-Cl}

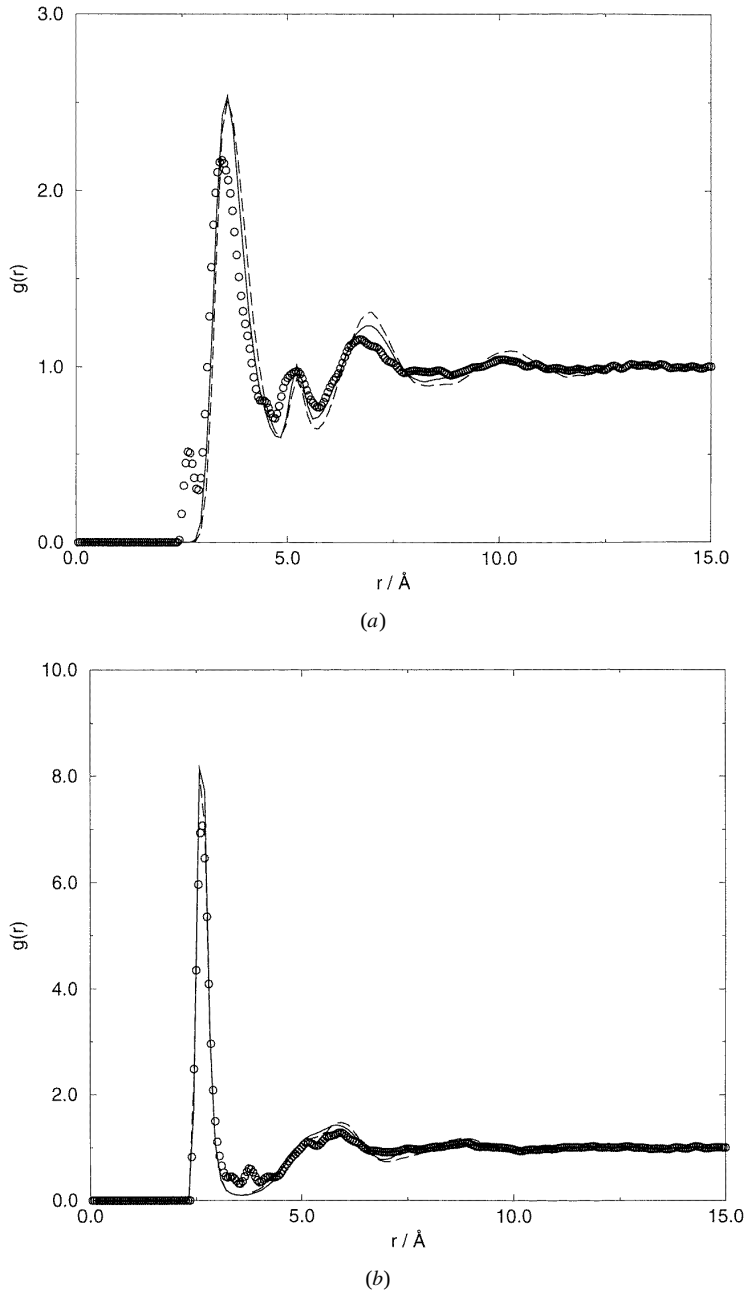

Figure 1. Comparison of the partial rdfs obtained with the PIM and the RIM potentials along with those obtained from Fourier transforms of the experimental neutron partial structure factors for the pure molten $DyCl_3$. In each case, the solid curve is the RIM result, the dashed curve is the PIM result and the open circles represent the experimental data. (*a*) Cl–Cl correlation, (*b*) Dy–Cl correlation and (*c*) Dy–Dy correlation.

and $g_{\mathrm{Cl-Cl}}$ are predicted to have very similar shapes in the RIM and PIM simulations, which indicates that the spatial distribution of the anions is little affected by the polarization effects.

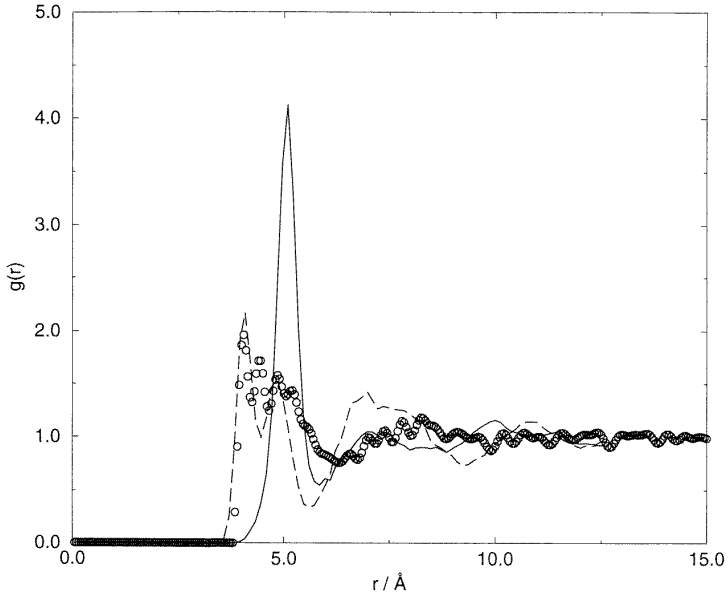

(*c*)

Figure 1. (Continued)

In both cases, the predicted rdfs agree well with the experimental ones. The mean coordination number of Cl^- around Dy^{3+} (obtained by integrating g_{Dy-Cl} up to 3.5 Å) is found to be 6 and the distribution of Cl–Dy–Cl bond angles is consistent with octahedral coordination. The first peak in g_{Cl-Cl} is due to Cl^- ions which are adjacent in the octahedral unit, whereas the small second peak, at ∼5.3 Å, is due to pairs of Cl ions which lie at opposite vertices of the octahedron, and is therefore at twice the distance of the first peak of g_{Dy-Cl}. The fact that g_{Dy-Cl} remains at a finite value at its first minimum suggests that the octahedral coordination is not rigid; there is some exchange of Cl^- ions between the coordination shell and the bulk.

Despite the similarity of g_{Dy-Cl} and g_{Cl-Cl} in the PIM and RIM simulations, the results for g_{Dy-Dy} in the two simulations are very different. This indicates that, as has been found for MX_2 systems [16], anion polarization has a major effect on the way the local coordination polyhedra (octahedra in this case) are connected together, since the connectivity strongly affects the distance of closest approach of the cations. The PIM result for g_{Dy-Dy} is very similar to that obtained experimentally. The first peak is very broad and appears to be split into two peaks (as do the experimental data); the first of these at ∼4.0 Å strongly overlaps the first peak of g_{Cl-Cl}. One would instinctively expect that the strong Coulomb repulsion between Dy^{3+} ions would force them to larger separation than for Cl^-–Cl^-. For the RIM, the first peak of g_{Dy-Dy} conforms to this expectation, since it lies in the first minimum of g_{Cl-Cl} and it is very sharp, implying that it is determined by strong repulsive interactions. It is noteworthy that the second component of the first peak in the PIM (and experimental) g_{Dy-Dy} appears at roughly the same radial position (slightly shorter). We experimented with many combinations of RIM potential parameters but invariably failed to reproduce the shape of g_{Dy-Dy} observed experimentally.

The origin of the difference between the RIM and PIM predictions for g_{Dy-Dy} is the fact that the Coulombic repulsion between the cations, which tends to maximize their separation, is offset by anion polarization effects, which tends to bend the Dy–Cl–Dy bonds [2]. For local octahedral coordination, the Coulombic repulsion favours a connection of octahedra via

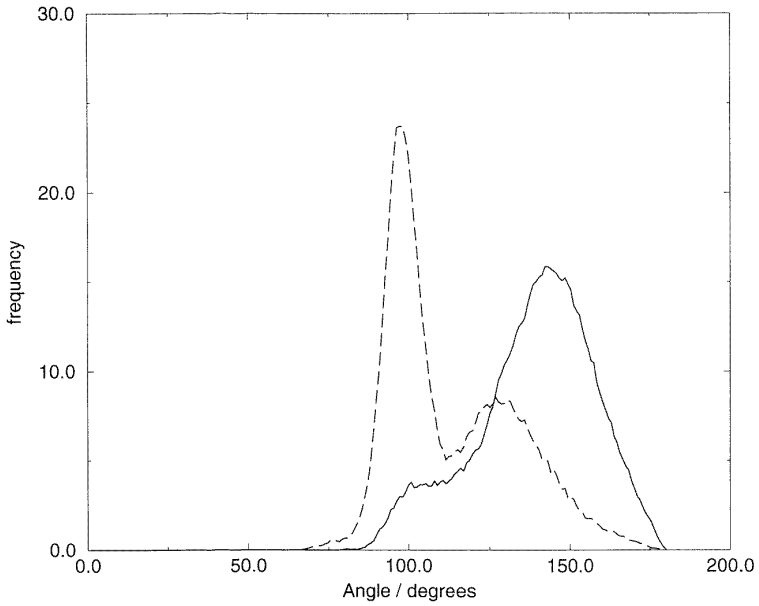

Figure 2. Angular distribution of Dy–Cl–Dy linkages in the pure molten $DyCl_3$ for the RIM potential (solid curve) and the PIM potential (dashed curve).

a corner-sharing arrangement with a nearly linear Dy–Cl–Dy 'bond'. Polarization effects promote the bending of the bond for a corner-sharing arrangement, and may also promote the formation of edge-sharing connections between the octahedral units. This is illustrated in figure 2 where the Dy–Cl–Dy bond-angle distributions are shown for the PIM and RIM calculations. Both show two features, corresponding to bond angles below and above 100°, respectively. We associate the larger-angle feature with octahedral corner sharing: note that the intensity of this feature is lower in the PIM calculations and is shifted to smaller angles than in the RIM, indicating a reduction in the extent of corner sharing and a bending of the bond. The small-angle feature is due to edge-sharing octahedra, and it dominates the distribution in the PIM calculations. We may now understand the double peak of the first feature in the PIM and experimental $g_{\mathrm{Dy-Dy}}$. The peak at the very small separation is associated with the edge-sharing units, with the two cations brought into close proximity by the edge sharing. The second peak is due to residual corner-sharing units. Here the Dy–Dy separation is close to—but slightly smaller than—that seen in the RIM; the reduction is brought about by the bending of the Dy–Cl–Dy bond. A detailed analysis of the network structure shows only a small number of face-sharing units. Instantaneous configurations of $DyCl_3$ are shown in figures 3(*a*) and 3(*b*) for the PIM and RIM systems, respectively.

3.2. Reciprocal-space structure

In MX_2 systems, the polarization-induced reduction in the nearest-neighbour separation of the cations is associated with the development of a pre-peak or first sharp diffraction peak in the structure factors observed in neutron and x-ray scattering experiments [16]. The development of such a feature is regarded as the signature of non-trivial intermediate-range order in the network formed through connection of the coordination polyhedra [17]. In figure 4 we show the total neutron structure for $DyCl_3$ [12], observed for the natural isotopic abundances, and

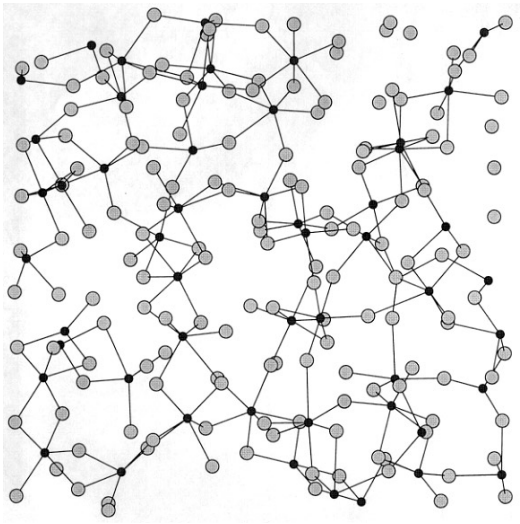

(*a*)

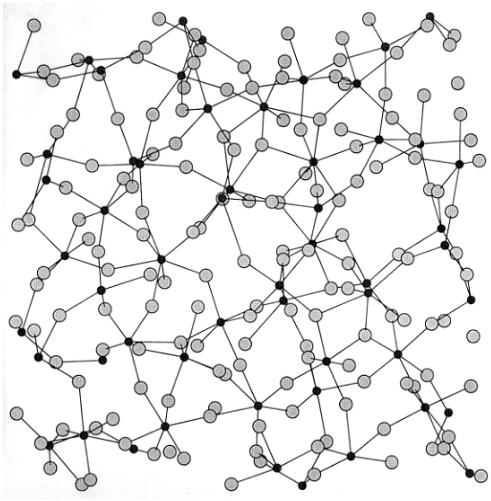

(*b*)

Figure 3. Slices through instantaneous configurations of pure molten $DyCl_3$ for (*a*) the PIM and (*b*) the RIM systems.

as calculated using the RIM and PIM. A prominent pre-peak is seen in the PIM result. Its position and height are in very good accord with the experimental pre-peak. There is also a pre-peak present in the RIM result, though it is shifted to slightly larger k-values.

Overall, the agreement between the calculated total structure factor and experiment appears not as good as indicated above for the individual partial rdfs. This apparent paradox can be resolved by noting, as shown by the neutron-weighted partial contributions in the inset to figure 4, that the shape of the total structure factor is crucially affected by cancellation between the different components, especially in the vicinity of the principal peak.

Thus, very small shifts in the positions of features in real space, or an underestimate of the extent of long-range order, whilst producing small effects at the level of the partials, can

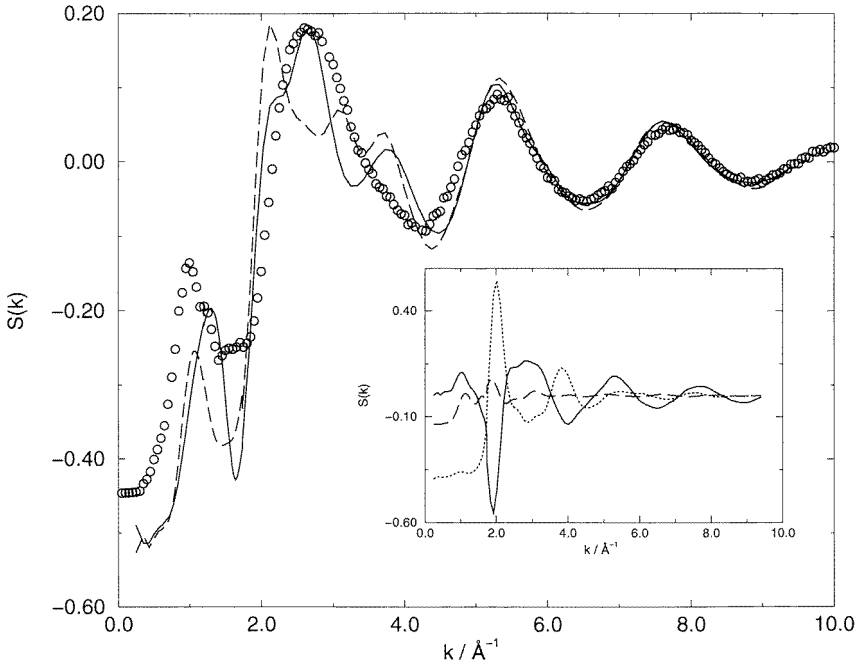

(*a*)

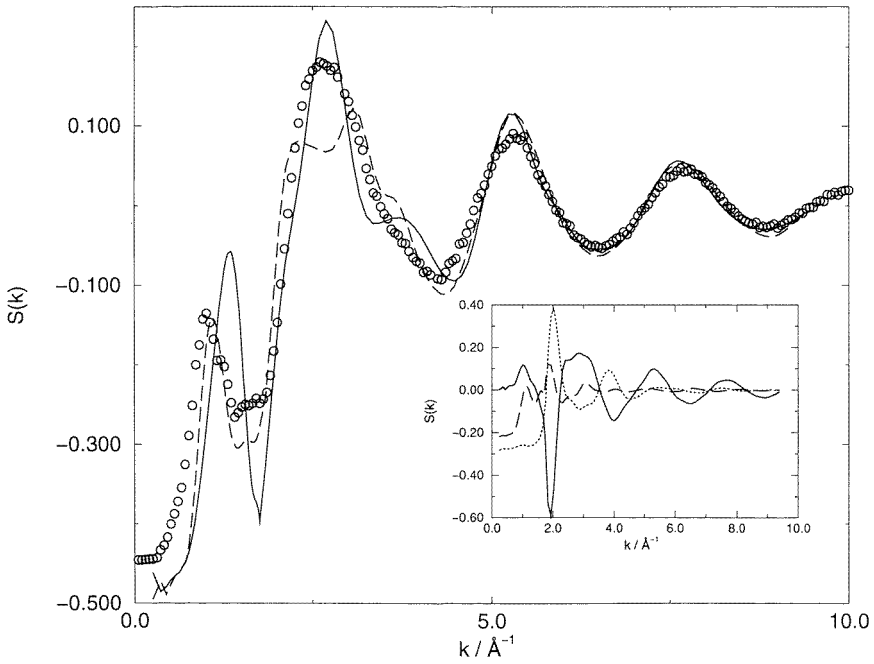

(*b*)

Figure 4. Comparison of total neutron-weighted structure factors for the pure molten $DyCl_3$ obtained from the RIM potential (solid curve), the PIM potential (dashed curve) and the experiment (open circle) for two different scattering lengths. The inset to the figure shows the neutron-weighted partial contributions. Cl–Cl partial $S(k)$ is the dotted curve, Dy–Cl partial $S(k)$ is the solid curve and Dy–Dy partial $S(k)$ is the dashed curve. (*a*) $b(Dy^{3+}) = 16.9$ fm and (*b*) $b(Dy^{3+}) = 25.2$ fm.

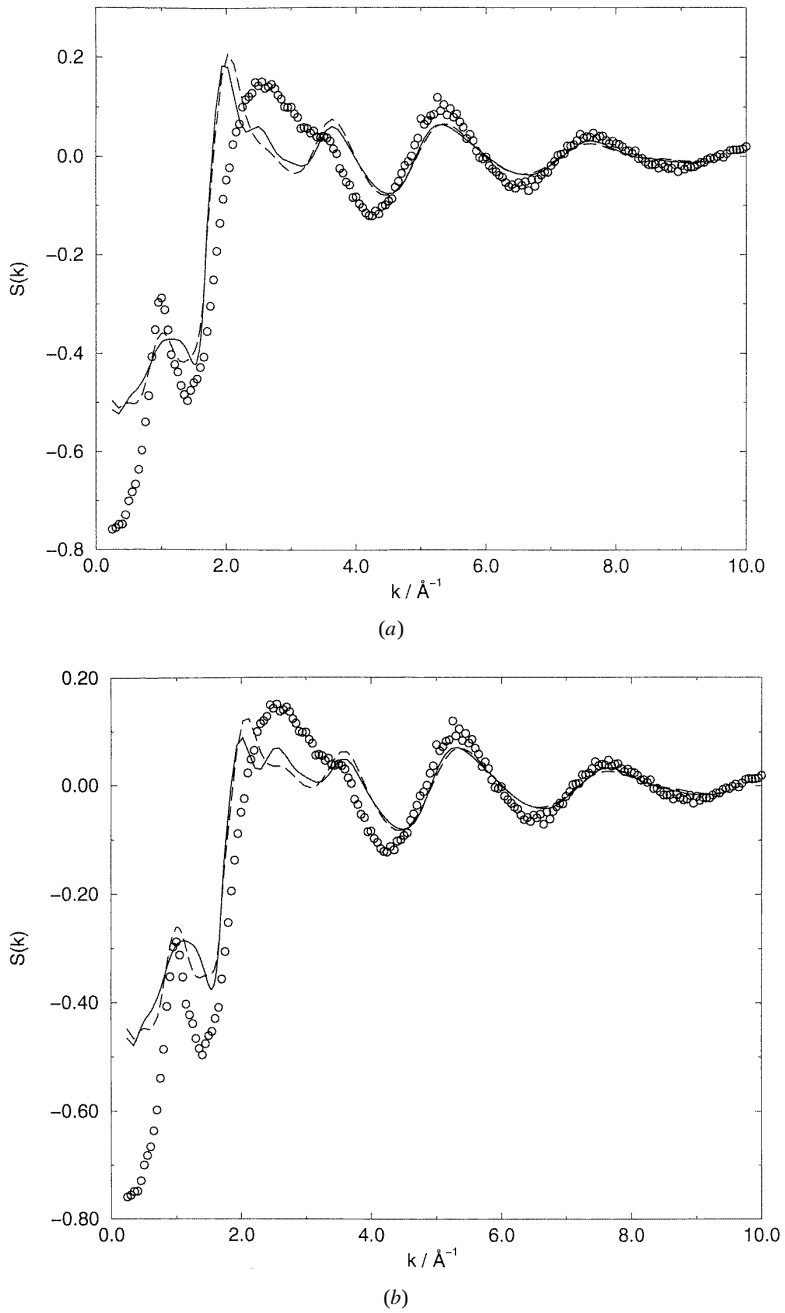

Figure 5. Comparison of the total neutron-weighted structure factors for the molten $DyNa_3Cl_6$ for two different Dy^{3+} scattering lengths. The solid curve represents the result for the RIM potential, the dashed curve is the result for the PIM potential and the open circles represent the experimental data. (*a*) $b(Dy^{3+}) = 16.9$ fm and (*b*) $b(Dy^{3+}) = 25.2$ fm.

impose major changes on the shape of $S(k)$. The scattering length of Dy^{3+} which, due to nuclear resonances, varies quite considerably as a function of the wavelength used, also affects

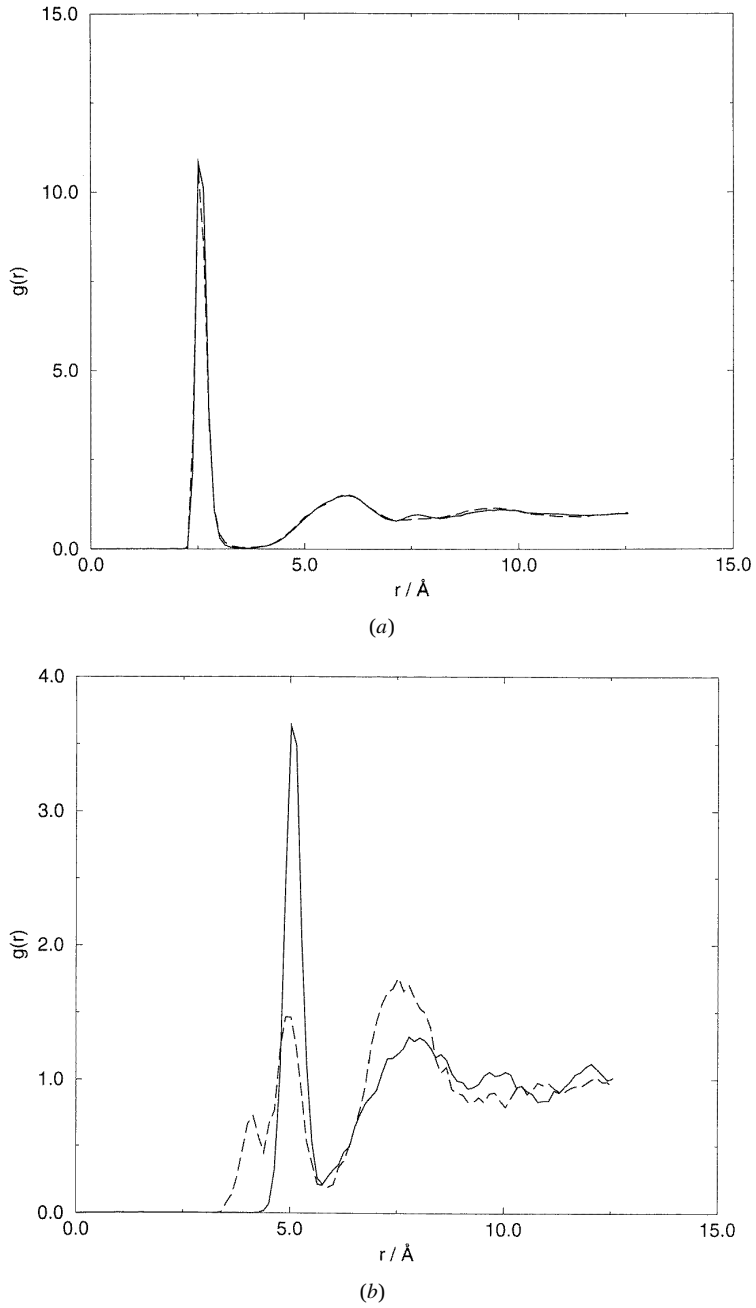

Figure 6. Partial rdfs for several ionic configurations in molten $DyNa_3Cl_6$. The PIM result is represented by the dashed curves and the RIM result is represented by the solid curves. (*a*) Dy–Cl correlation. (*b*) Dy–Dy correlation. (*c*) Dy–Na correlation. (*d*) Na–Na correlation.

the shape of the total structure factor. This variation is shown in figures 4(*a*) and 4(*b*). In figure 4(*a*) the coherent scattering length of Dy(natural) is 16.9 fm [18], while in figure 4(*b*) it was accidentally estimated to be 25.2 fm.

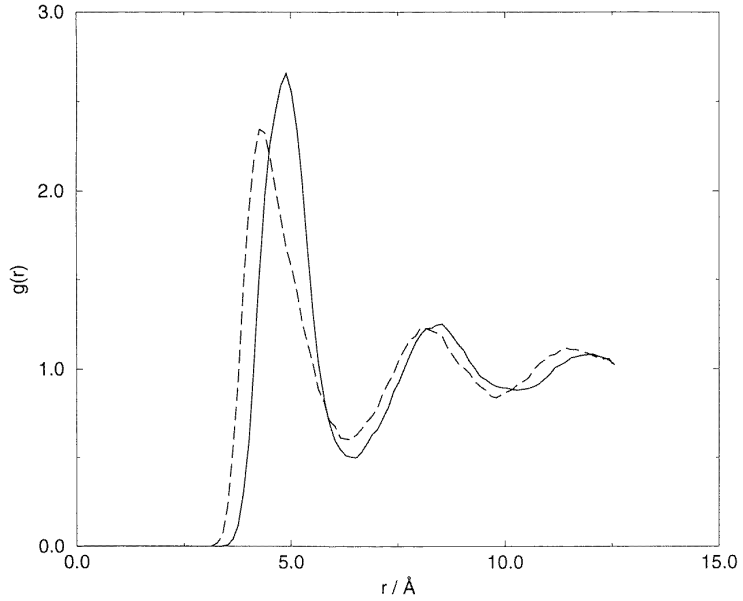

(*c*)

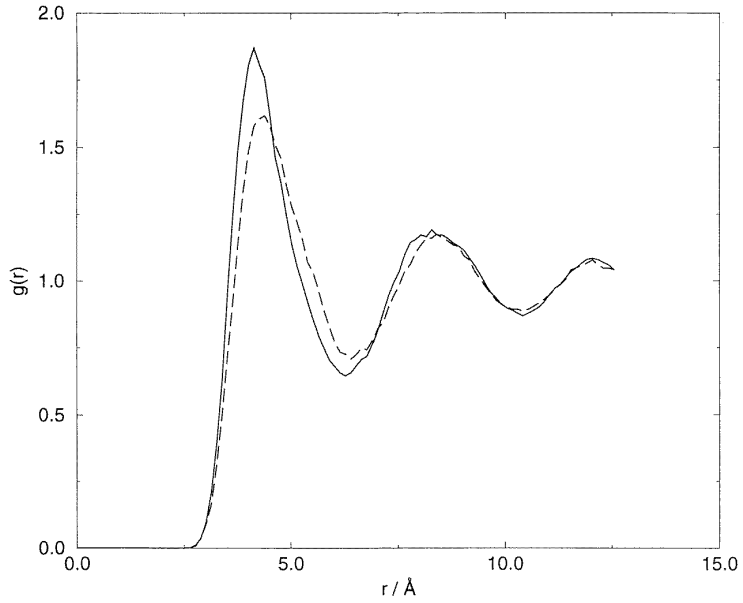

(*d*)

Figure 6. (Continued)

4. Results for $DyNa_3Cl_6$ mixture

In network-forming ionic liquids, it is commonly observed that addition of a salt with a common anion in combination with a weakly coordinating cation breaks down the network structure [19, 20]. This process is of some technological significance, as it plays an important role

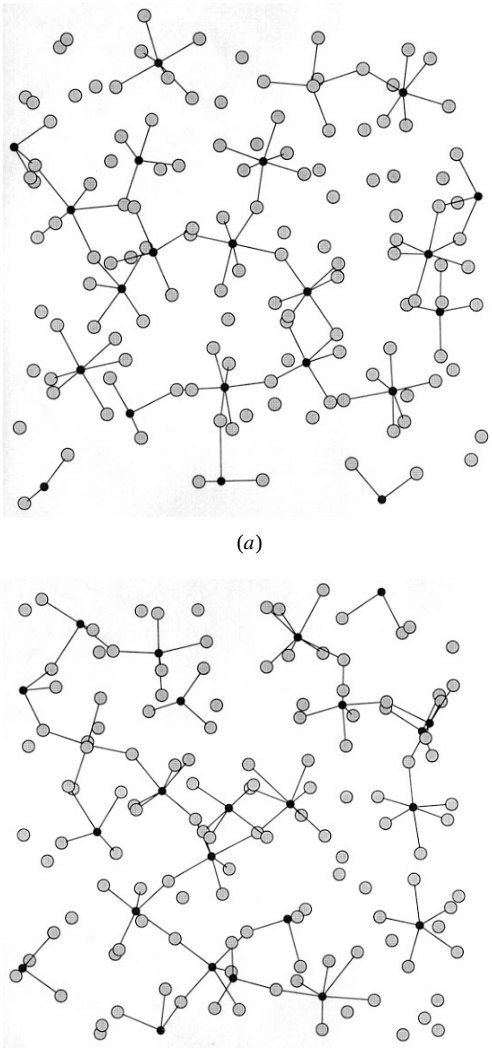

Figure 7. Slices through instantaneous configurations of $DyCl_6^{3-}$ for (*a*) PIM and (*b*) RIM systems in $DyNa_3Cl_6$.

in the refinement and extraction process. It is of interest to see how addition of NaCl to form a mixture of stoichiometry $DyNa_3Cl_6$ affects the Dy–Cl coordination. Thermodynamics indicates compound formation at this stoichiometry. The enthalpy of mixing of molten $DyCl_3$–NaCl shows a minimum around a $DyCl_3$ content of 25% [21], where the concentration of Cl^- ions is sufficient to isolate $DyCl_6^{3-}$ complexes. Similar studies on the dissolution of $ZnCl_2$ in alkali halides with the PIM have been made previously [20]. In the previous section, we have shown that the PIM reproduces distinctive structural properties of pure $DyCl_3$ rather well. We now combine this with pair potentials which describe the Na–Na and Na–Cl interactions taken from [22]. The Dy–Na interaction is dominated by simple Coulomb repulsion.

Total structure factors ($S_{\text{total}}(k)$) estimated by MD simulations with the PIM and RIM interaction models are depicted in figure 5 together with the experimental total structure factor.

$S_{\text{total}}(k)$ estimated using the PIM is quite similar to the experimental one, especially beyond $\sim$3.5 Å^{-1}. The height and location of the first sharp diffraction peak estimated using the PIM shows good agreement with the experimental results. It seems reasonable to say that $S_{\text{total}}(k)$ obtained with the PIM is better than that obtained with the RIM at low k.

In figures 6(*a*)–6(*d*), partial rdfs of several ionic combinations in the mixture are shown. $g_{\text{Dy-Cl}}$ is similar in the two simulations, with a sharply defined first coordination shell which integrates to six nearest neighbours. In contrast to the case for the pure melt, the first minimum in $g_{\text{Dy-Cl}}$ now goes to zero, indicating a very stable coordination complex from which Cl^- ions exchange very slowly with the bulk. Significant differences between the PIM and RIM predictions appear in $g_{\text{Dy-Dy}}$. Since there is a peak at around 5.0 Å in $g_{\text{Dy-Dy}}$ (RIM), similar to the positioning of the first peak in the pure $DyCl_3$ simulations, it appears that there are dimers or bigger polymers of connected polyhedra. On the other hand, the most prominent peak in $g_{\text{Dy-Dy}}$ in the PIM simulation is at much larger separation, suggesting that Dy^{3+} ions and their immediate coordination neighbours have become disconnected. It would appear that the polarization effects have promoted the break-up of the network and the formation of discrete $DyCl_6^{3-}$ molecular ion units. In figures 7(*a*) and 7(*b*), views of instantaneous configurations of $DyCl_6^{3-}$ are depicted for the PIM and RIM systems, respectively. In these figures only the positions of Dy^{3+} ions (dark circles) and Cl^- ions are shown, along with lines connecting Cl^- ions coordinating to the Dy^{3+} ions. One can see how uniformly $DyCl_6^{3-}$ complexes distribute in the PIM simulation. Ideal octahedral coordination is realized in both of the PIM and RIM systems. Na^+ ions have to coordinate with Cl^- ions rigidly coordinated to Dy^{3+}, so an interaction distance (4.0 Å) between Dy^{3+} and Na^+ in the PIM system is shorter than that (5.0 Å) in the RIM system. Other interactions (Dy–Cl, Na–Cl and Cl–Cl) are similar in both of the PIM and RIM systems. As expected, there are different cation–cation interactions between the PIM and RIM systems.

5. Conclusions

MD simulations of the molten $DyCl_3$ were performed with the PIM and RIM, where the same potential parameters were employed. In the PIM the polarization of Cl^- ions was supplemented. While in the both systems $g_{\text{Dy-Cl}}(r)$ and $g_{\text{Cl-Cl}}(r)$ are very similar, $g_{\text{Dy-Dy}}(r)$ for the PIM system shows a shorter interaction distance than that of the RIM system. This shorter interaction distance is observed in the experimental rdf determined with the isotopic substitution method. It is concluded that strong Coulomb interaction between Dy^{3+} and Dy^{3+} is screened by the polarization of Cl^- ions.

On the other hand, MD simulation of $DyNa_3Cl_6$ with the PIM shows that the most prominent peak of $g_{\text{Dy-Dy}}(r)$ is at much larger separation. It would appear that the polarization effects have promoted the break-up of the network and the formation of discrete $DyCl_6^{3-}$ molecular ion units.

References

[1] Tatlipinar H, Akdeniz Z, Pastore G and Tosi M P 1992 *J. Phys.: Condens. Matter* **4** 8933
[2] Madden P A and Wilson M 1996 *Chem. Soc. Rev.* **25** 339
[3] Stone A J 1996 *The Theory of Intermolecular Forces* (Oxford: Clarendon)
[4] Wilson M, Madden P A and Costa-Cabral B J 1996 *J. Phys. Chem.* **100** 1227
[5] Wilson M, Madden P A, Pyper N C and Harding J H 1996 *J. Chem. Phys.* **104** 8068
[6] Wilson M and Madden P A 1994 *J. Phys.: Condens. Matter* **6** 159
[7] Wilson M and Madden P A 1994 *Phys. Rev. Lett.* **72** 3033
[8] Wilson M and Madden P A 1993 *J. Phys.: Condens. Matter* **5** 2687

[9] Wilson N T, Wilson M, Madden P A and Pyper N C 1996 *J. Chem. Phys.* **105** 11 209
[10] Saboungi M-L, Price D L, Scamehorn C and Tosi M P 1991 *Europhys. Lett.* **15** 283
[11] Mochinaga J, Iwadate Y and Fukushima K 1991 *Mater. Sci. Forum* **73–75** 147
[12] Adya A K, Takagi R, Sato Y, Gaune-Escard M, Barnes A C and Fischer H 1999 to be submitted
[13] Pyper N C 1991 *Adv. Solid State Chem.* **2** 223
[14] Fowler P W and Madden P A 1984 *Phys. Rev.* B **29** 1035
[15] Igarashi K and Mochinaga J 1987 *Z. Naturf.* a **42** 777
[16] Wilson M and Madden P A 1998 *Phys. Rev. Lett.* **80** 532
[17] Price D L, Moss S C, Reijers R, Saboungi M-L and Susman S 1989 *J. Phys.: Condens. Matter* **1** 1005
[18] Mughabghab S F, Divadeenam M and Hulden N E 1981 *Neutron Resonance Parameters and Thermal Cross Sections (Neutron Cross Sections vol 1)* (New York: Academic)
[19] Papatheodorou G N 1977 *J. Chem. Phys.* **66** 2893
Papatheodorou G N 1977 *J. Inorg. Nucl. Chem. Lett.* **11** 483
[20] Pavlatou E A, Madden P A and Wilson M 1997 *J. Chem. Phys.* **107** 10 446
[21] Takagi R, Rycerz L and Gaune-Escard M 1994 *Denki Kagaku* **62** 240
[22] Sangster M J L and Dixon M 1976 *Adv. Phys.* **23** 247